Reviews of Modern Plasma Physics (2026) 10:13
https://doi.org/10.1007/s41614-026-00223-z

REVIEW PAPER

Reduction of graphene oxide flakes by treatment with non-equilibrium hydrogen plasma–review and challenges

František Zelenak[1] · Richard Krumpolec[1] · Dušan Kováčik[1] · Rok Zaplotnik[2] · Alenka Vesel[2] · Gregor Primc[2] · Miran Mozetič[2]

Received: 26 January 2026 / Accepted: 14 June 2026

Abstract

Graphene oxide (GO) is a standard precursor for the synthesis of porous yet densely packed, graphene-like structures in films with a thickness of several micrometers, which are useful for electrodes in various electrochemical devices, such as supercapacitors, as well as for various sensors. As-synthesized GO films exhibit inadequate electrical conductivity because of a large concentration of oxygen chemically bonded to graphene sheets. Heating of GO films in a non-oxidizing atmosphere will cause thermal decomposition of GO by desorption of carbon oxides, which will result in numerous defects in the sheets and partial collapsing of the sheets. An alternative is the treatment of GO films with non-equilibrium hydrogen plasma, which causes reduction rather than decomposition of the GO sheets. The scientific literature on approaches to reducing GO samples by treatment with hydrogen plasma is reviewed, the results are critically evaluated, and the correlations between the reduction efficiency and processing parameters are drawn. Paradoxically, larger discharge powers lead to worse results, both in terms of the remaining oxygen concentration and electrical properties. A feasible explanation for this paradox is radiation damage, which is likely caused by energetic photons or ions. The recommendation for further experiments in this tremendously promising niche is also presented.

Keywords Graphene oxide · Graphene oxide reduction · Plasma reduced graphene oxide · Hydrogen plasma

✉ František Zelenak
frantisek.zelenak@mail.muni.cz

[1] Faculty of Science, Department of Plasma Physics and Technology, CEPLANT—R&D Center for Plasma and Nanotechnology Surface Modifications, Masaryk University, Kotlářská 267/2, Brno 602 00, Czech Republic

[2] Department of Surface Engineering, Jožef Stefan Institute, Jamova cesta 39, Ljubljana 1000, Slovenia

Published online: 26 June 2026

1 Introduction

Carbon materials with a large surface-to-mass ratio have attracted significant attention from the scientific community due to their promising applications. The high surface-to-mass ratio is attributed to highly porous structures or specific morphological features, such as fullerenes, nanotubes, nanorods, and nanowalls. A material of particular interest is a single-layer hexagonal carbon flake, commonly referred to as graphene. Graphene exhibits outstanding electrical and mechanical properties as long as the properties are normalized to the mass.

There are several techniques for synthesizing graphene sheets. The exfoliation of highly oriented pyrolytic graphite (HOPG) is probably the simplest. (Novoselov et al. 2004). Another technique is the deposition of a carbon monolayer from the vapor phase onto a suitable substrate such as copper foil (Gallo et al. 2012). These techniques are beneficial for studying the fundamental properties of graphene functionalized with various dopants; however, they lack scalability for industrial applications. That is because carbon materials with a large surface-to-mass ratio should be three-dimensional on the macroscopic scale to be useful for applications such as energy storage devices, catalysts, membranes, etc. A valuable technique for depositing graphene films with relatively large thickness on a macroscopic scale is chemical vapor deposition (CVD). Under a limited range of experimental conditions, graphene sheets grow perpendicularly to the substrate surface, forming a film with a thickness exceeding 1 μm (Wang et al. 2004; French et al. 2006). This technique was elaborated by several researchers worldwide, but the synthesized structures were not dense enough to enable optimal material for supercapacitors or similar devices. In such devices, the preferred distance between neighboring graphene sheets should be a few nanometers, but the vast majority of authors who have used CVD for the deposition of graphene sheets have reported much larger distances, often in the order of 100 nanometers (Vesel et al. 2019). Such large distances enable the penetration of ionic liquids into the gaps between neighboring sheets; however, the specific capacitance of electric double-layer capacitors is inferior due to this large distance.

An alternative to CVD deposition of graphene sheets is the synthesis of graphene oxide (GO) sheets, followed by their reduction to a graphene-like material referred to as reduced graphene oxide. GO is relatively easy to synthesize in large quantities through liquid-phase exfoliation (Hofmann 1928; Hummers and Offeman 1958; Park et al. 2017; Gurzęda et al. 2024). This technique has been used for decades and it enables the synthesis of GO sheets of appropriate dimensions, provided the synthesis procedure is optimized (Huskić et al. 2024). The GO sheets, however, do not exhibit adequate electrical conductivity due to the large concentration of oxygen that disrupts the sp^2 hybridization of the graphene lattice (Jung et al. 2008). The requirements for energy storage devices would be met if the GO sheets in the macroscopic films were reduced, i.e., oxygen removed from the graphene structure without significant damage to the hexagonal structure and without significantly altering the distance between neighboring sheets. Such an ideal case is illustrated in Fig. 1.

As-synthesized GO is thermally unstable and will spontaneously decompose at elevated temperatures in the absence of strong oxidants (Becerril et al. 2008). However, such a reduction causes at least partial degradation of the sheets (Akbi et al.

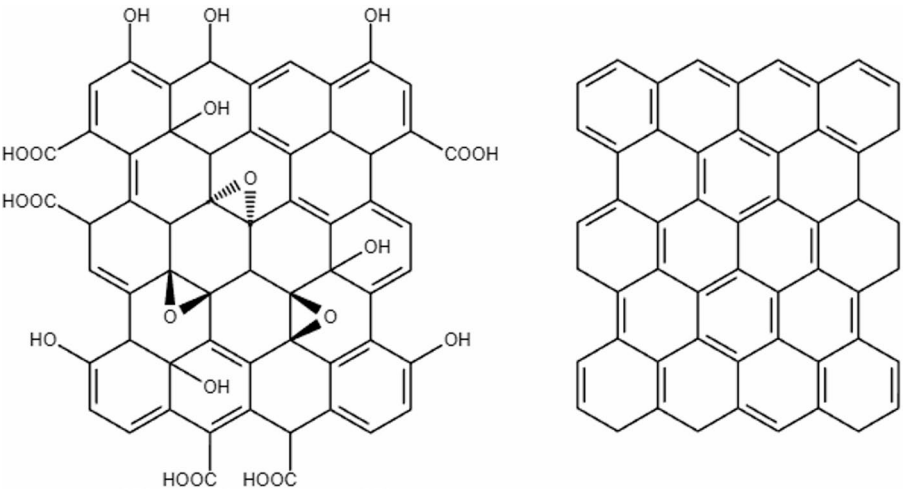

Fig. 1 Schematic representation of an ideal case for the reduction of graphene oxide; **a** as-synthesized GO; **b** the GO after reduction

2023). Furthermore, the heating in the protective atmosphere never leads to complete reduction. This is because, after heating GO sheets in a protective atmosphere, the oxygen concentration remains 10–20 at%, and the electrical or thermal conductivity remains moderate (Acik et al. 2011; Sengupta et al. 2018; Seon Lee et al. 2024).

A popular method for reducing virtually any oxide is the application of thermodynamically non-equilibrium hydrogen plasma (Janca et al. 2003; Jovičević-Klug et al. 2024; Zhang et al. 2025). Various electrical discharges could sustain hydrogen plasma. Several authors who investigated the reduction of graphene oxide employed low-pressure discharges, while a few preferred atmospheric-pressure discharges. There is a vast difference between low-pressure and atmospheric pressure plasmas (Primc et al. 2022), with the most relevant aspect for GO reduction being that reactive species are lost in the gas phase at atmospheric pressure, whereas they are lost only on surfaces at pressures below a few mbar (Primc 2022). Obviously, low-pressure plasmas are more energy-efficient, so most authors have used them for GO reduction. Other advantages of using low-pressure plasmas are explained in (Mozetič 2025).

Different discharges could sustain low-pressure non-equilibrium hydrogen plasma. Radiofrequency (RF) discharges are most popular, but some authors also used microwave discharges. RF discharges could be sustained in different modes (Zaplotnik et al. 2021), and specifics dictate the flux of reactive species on the surface of the GO samples. The species include positively charged hydrogen ions, neutral atoms in the ground electronic states, and energetic photons (Fantz et al. 2016). The interaction between these species and graphene oxide is illustrated in Fig. 2. All particles in the gas phase, i.e., those far away from any surface, move randomly, and their velocity depends on the gas temperature and the particle mass. The average random velocity is:

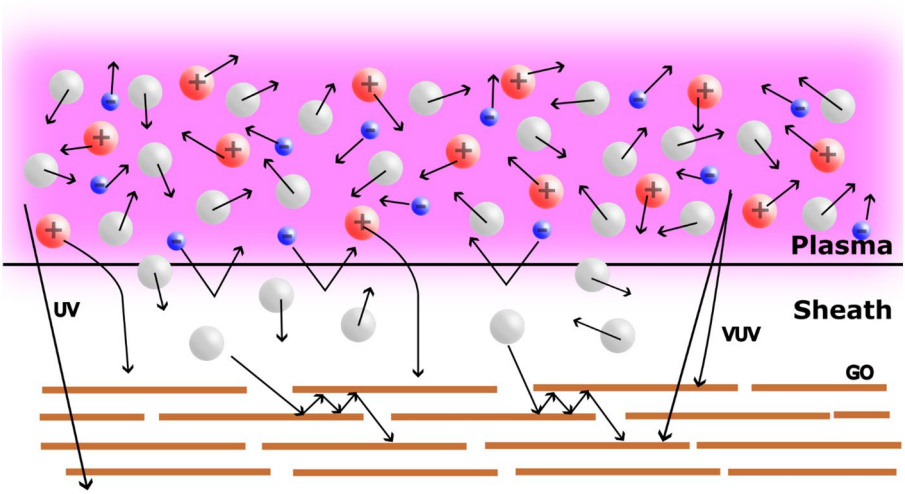

Fig. 2 Illustration of the interaction of species formed in hydrogen plasma with a film of GO or reduced GO composed of numerous flakes when the samples are at the floating potential. Not to scale

$$< v > = \sqrt{\frac{8k_B T}{\pi\, m}} \tag{1}$$

where k_B is the Boltzmann constant, T is the gas temperature, and m is the particle mass. The kinetic energy is:

$$E_k = \frac{m< v >^2}{2} \tag{2}$$

The average velocity $<v>$ of positively charged ions and neutral molecules is practically the same in the gas phase because of the abundance of elastic collisions, which are responsible for sharing the kinetic energy between charged and neutral hydrogen molecules or atoms. Ions are not significantly accelerated in high-frequency discharges because of the simple fact that massive particles cannot follow the fast oscillations of the electric field. On the other hand, electrons can follow the oscillations of the electric field (Chen et al. 2004). The space charge in plasma reactors causes the electric field to shrink to a rather narrow layer next to the solid materials. If the surface of the solid material is powered with an RF generator, a DC self-bias of several 100 V occurs next to the powered electrode (which may be covered with a thin film of an insulator without significant disturbance of the electric field) (Yonemura et al. 2006). The electrons emitted from the solid material accelerate in such a strong electric field and do not lose much energy at elastic collisions with other particles, so their temperature in a non-equilibrium plasma is much larger than the gas temperature. Typically, the electron temperature is several 10,000 K, and the gas temperature is several 100 K. Considering Eq. (1), the electron velocity will be about 10 times larger than the velocity of any other particle, just because of the different temperatures. The main reason for the large velocity of the electrons, however, is the

huge mass difference. The mass of a hydrogen atom is 3 orders of magnitude larger than the electron mass. Considering both the temperature and the mass difference, the electron velocity as calculated from Eq. (1) will be over 100 times larger than the ion velocity in the unperturbed plasma. This large velocity causes electrons to escape from the gas phase, accumulating on all surfaces that face the plasma and leaving positively charged ions in the gas phase. The negative surface charge appears almost immediately after the discharge is turned on, preventing many plasma electrons from reaching the surface. The potential drop between plasma and the surface of a solid material will also accelerate ions toward the surface. The sheath thickness between the plasma and the surface, not backed by an electrode, in non-equilibrium low-pressure hydrogen plasma is of the order of the Debye length, typically ranging from a few tens of micrometers to a few hundred micrometers (Mozetič et al. 2019). The Debye length is inversely proportional to the square of the electron density.

The sheath between the unperturbed plasma and a material immersed in plasma dictates the interaction of charged particles with the solid material. If the GO flakes are rather densely packed in the film to be treated by hydrogen plasma and the distance between the neighboring flakes is smaller than the sheath thickness, the charged particles would not recognize the morphological properties of the GO film. This means that the majority of plasma electrons will not reach the surface, and those from the high-energy tail will reach the surface with low kinetic energy. Obviously, electrons are not capable of causing any surface reaction when material is exposed to non-equilibrium low-pressure hydrogen plasma. On the other hand, the ions will be accelerated in the sheath next to the sample and will bombard the surface of the uppermost GO flakes. The probability for surface neutralization of charged particles is practically 100% (Economou et al. 2009), so the ions will be neutralized once they touch the surface. If the sample is at a floating potential, the voltage across the sheath will be only up to a few tens of eV (Mozetič et al. 2019). Conversely, if the sample is biased, the voltage will be almost as large as the discharge voltage, provided the biased electrode is much smaller than the counter electrode.

Neutral atomic hydrogen atoms are chemically reactive but do not react to any electric field, so they move randomly both in the plasma and the sheath, as well as in the gaps between the neighboring flakes. They could be lost on the surface through a chemical reaction or heterogeneous recombination. The recombination coefficient for smooth graphite materials is of the order 10^{-3} (Drenik et al. 2011; Petucci et al. 2018). The H atoms will thus penetrate well into the space between the neighboring flakes within a GO film, as illustrated in Fig. 2. Hydrogen plasma causes slow chemical etching of carbon materials (Long et al. 2020).

The spectra of hydrogen plasma are presented in classical literature (Fantz et al. 2016). The vast majority of radiation falls within the vacuum ultraviolet range, i.e., between approximately 110 and 200 nm, corresponding to photon energies between 11 and 6 eV. The penetration depth of photons emitted from a hydrogen plasma into graphene sheets has yet to be determined. Pure single-layer graphene is practically transparent to visible radiation (Nair et al. 2008). Films of densely packed graphene are visually black, meaning that the most photons in the visible range are absorbed. The penetration depth of UV-C and VUV photons in multilayer graphene flakes should be somewhere between that of a single-layer graphene and a thick film of

densely packed graphene sheets. As shown in Fig. 2, the photons from the hydrogen plasma are likely to penetrate through the uppermost flakes, but not deep into the film.

This introduction to hydrogen plasma reveals that the interaction with hydrogen atoms is purely chemical because of the negligible kinetic energy of atoms impinging on the surface. Unlike atoms. the ions carry both potential energy (ionization energy) and kinetic energy (acquired across the sheath), and these energies are similar in plasmas with an electron temperature of a few eV, provided the samples are at floating potential. Negative biasing will increase the ion energy. The interaction of photons cannot be neglected because the major radiation is in the VUV range, so photons have energy larger than the binding energy between carbon atoms in the graphene or graphene oxide structure. The photons probably penetrate more than a few monolayers deep into the GO structure.

2 Literature survey

2.1 Low-pressure treatment

As illustrated in Fig. 2, the treatment of films composed of graphene sheets with hydrogen plasma will cause modification of not only the flakes on the surface, but also the flakes distributed inside a thicker film of packed GO flakes. Therefore, the treatment is effective in reducing the uppermost GO flakes and those packed deeper within the film, provided that hydrogen atoms and UV/VUV radiation can reach them. The reduction of GO by hydrogen plasma treatment attracted the attention of several authors, and the most significant results are summarized and critically evaluated in this review article.

One of the first reports of GO hydrogen plasma reduction at room temperature was by Hafiz et al. (2014). They synthesized the GO flakes using a simplified Hummers method. The flakes were spin-coated onto silica substrates, which were mounted on a grounded electrode in a capacitively coupled RF discharge. They used a home-made system illustrated in Fig. 3. The discharge chamber was metallic and grounded, so practically all discharge power was dissipated near the powered electrode in such a strongly asymmetric RF discharge. The remaining discharge volume was occupied

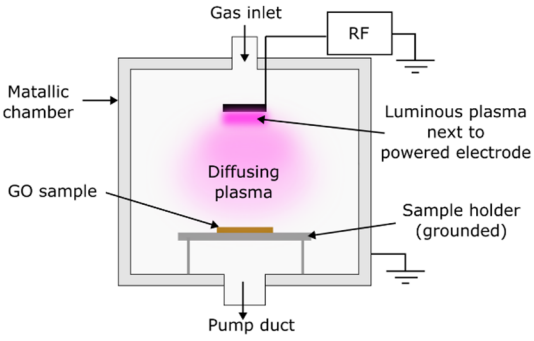

Fig. 3 An illustration of the glass discharge tube for treating GO powder at low discharge power, as disclosed by Hafiz et al. (2014)

by a diffusing plasma, as illustrated in Fig. 3. The discharge was powered by an RF generator operating at the standard frequency of 13.56 MHz and with a discharge power of only 10 W. The gas pressure varied between 50 and 80 Pa, and the treatment times ranged from 20 to 40 s. The substrate holder temperature was measured with a thermocouple. As expected, the temperature rose by only a few K, even at the longest treatment time, which is explained by a small flux of H atoms on the sample surface. The small flux is due to a low discharge power and extensive loss of H atoms by recombination on the metallic surfaces of the discharge chamber (Melin et al. 1971). Another reason for marginal heating is a low coefficient of the surface association of H atoms to parent molecules on smooth carbon surfaces (Petucci et al. 2018). Interestingly enough, the authors mentioned the sputtering effect, which the bombardment with the energetic hydrogen ions might cause. However, the samples were practically at the floating potential (due to the huge difference in the areas of the powered and grounded metals facing the plasma), so the kinetic energy of the hydrogen ions was below the sputtering threshold. The interaction of the hydrogen plasma used by Hafiz et al. (2014) with their samples is evident in Fig. 3. The grounded electrode area was orders of magnitude larger than the powered electrode area. The samples were placed on the grounded electrode, so the effect of plasma treatment was essentially the same as if the samples had been kept at a floating potential. The morphology of the deposited flakes was evaluated using Scanning Electron Microscopy (SEM) and Atomic Force Microscopy (AFM), revealing that the flakes were composed of multilayer graphene sheets with an approximate thickness of 1 nm. The composition and structure of such flakes were determined by X-ray Photoelectron Spectroscopy (XPS). Untreated samples exhibited hydroxyl, carbonyl, and carboxyl functional groups. The concentration of all these groups decreased dramatically after the hydrogen plasma treatment. In fact, the concentration of the hydroxyl groups decreased below the detection limit when deconvoluting the high-resolution XPS C1s spectra. The final O/C ratio was 0.12. Such partially reduced GO flakes were found useful for use in gas-sensing devices.

Singh et al. (2014) reported the reduction of graphene oxide samples at room and elevated temperatures. The GO samples were prepared using Hummers' method. The authors used a DC discharge to sustain hydrogen plasma. The base pressure in the plasma reactor was approximately 10^{-4} Pa, and hydrogen leakage into the high-vacuum chamber allowed the pressure to reach 50 Pa. Other details about the experimental setup or the plasma parameters were not reported. The discharge power was 15–30 W, with treatment times up to 5 min and sample temperatures up to 120 °C. The morphology was probed using SEM and AFM, and the composition was analyzed by XPS. Unlike Hafiz et al. (2014), Singh et al. (2014) also reported the π-π shake-up satellite peak in the C1s spectra. The O/C ratio for untreated samples was 0.50, dropping to a value between 0.19 and 0.32 after hydrogen plasma treatment. Interestingly, Singh et al. (Singh et al. 2014) reported a significant concentration of hydroxyl groups even after hydrogen plasma treatment. In fact, the concentration of the C–O group, as revealed by the high-resolution C1s peaks, was 18% for untreated samples, and it ranged between 9 and 15% after plasma treatment. Observing such functional groups does not necessarily mean that the reduction was incomplete, but may be due to adventitious carbon adsorbed on the sample surface after plasma treat-

ment and before the samples are mounted in the XPS high-vacuum chamber (Grey et al. 2025). No straightforward correlation could be drawn between the plasma treatment time and the concentration of functional groups, as determined by XPS. Therefore, one may speculate that the concentration of adventitious carbon varied, possibly due to differences in the periods between the plasma treatment and the XPS measurements. The authors also probed different temperatures during the reduction and found no statistically significant differences up to 120 °C.

Jesuraj et al. (2018) prepared GO using the Hummers' method and spin-coated the suspension onto an Indium Tin Oxide (ITO) substrate that had been pretreated with oxygen plasma. The as-deposited films were heated to 120 °C for 15 min to remove the solvent. The gas pressure during hydrogen plasma treatment was approximately 40 Pa, and the discharge power was 15 W. The plasma was sustained by a DC discharge; however, the details of the experimental setup are not provided, so it cannot be determined whether the samples were at the floating potential or additionally biased negatively against the plasma. The as-deposited GO exhibited many C–O bonds, a marginal concentration of the C=O bond, and several atomic % of O=C–OH groups. The treatment with hydrogen plasma did not cause significant modification, as the high-resolution C1s peak was practically the same as that of untreated samples. This rather unexpected result was attributed to hydrogen-induced water formation in the treatment chamber. Another explanation mentioned by the authors is secondary oxidation resulting from exposure to ambient air between the plasma treatment and the XPS analysis. Yet a third explanation would be contamination with adventitious carbon (Grey et al. 2025).

Banerjee et al. (2018) deposited about 300 nm thick GO films by spin coating onto ITO substrates. The spreading solution contained commercially available GO flakes dispersed in water. The dry samples were treated for 30 min with hydrogen plasma sustained by an RF discharge. The hydrogen pressure was approximately 0.05 Pa, and the discharge power ranged from 20 to 60 W. Although no details about the plasma device are provided, according to the manufacturer, the plasma is sustained at a discharge power of approximately 50 W. The RF generator was operating at the standard frequency of 13.56 MHz. The plasma device is otherwise intended to remove traces of surface impurities before Transmission Electron Microscopy (TEM) analysis. The treatment of the GO films resulted in increased wettability of the samples, as evidenced by a decrease in the water contact angle from 115° to 100° after 30 min of plasma treatment and to 55° after 1 h of plasma treatment. A dramatic decrease in the optical band gap of the films was reported. In particular, it was 4.1 eV for untreated samples and 0.5 eV for samples treated for 60 min at 60 W discharge power. The conductivity of such plasma-treated films increased by 6 orders of magnitude. This represents the highest increase in conductivity reported by authors who reduced GO films via hydrogen plasma treatment. The authors found this technique beneficial for tuning the electrical and optical properties of elements used in flexible electronics.

Primo et al. (2018) synthesized GO flakes by the Hummers-Offeman method. The samples were partially reduced prior to hydrogen plasma treatment via hydrothermal reduction. Hydrogen plasma was sustained by a DC glow discharge in a glass chamber with planar electrodes, as illustrated in Fig. 4. The hydrogen pressure was 10 Pa. At such low pressure, the cathode dark space extends far from the cathode, and the

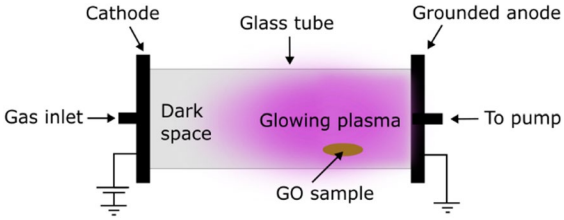

Fig. 4 An illustration of the glass discharge tube for treating GO powder at low discharge power, as disclosed by Primo et al. (2018)

rest of the discharge tube is occupied by a low-luminosity plasma. (Vesel et al. 2023). The discharge power depended on the voltage (values not reported in Primo et al. (2018) and ranged from 0.4 to 2 W. The samples were placed in the negative glow of the discharge as illustrated in Fig. 4, and the treatment time ranged from 15 to 60 min. Obviously, the samples were at floating potential at all times, so Fig. 2 well illustrates the interaction for this case, except that very low discharge power does not enable a significant concentration of plasma species, particularly not in the cathode dark space where hydrogen molecules are being introduced. The samples were characterized by Raman Spectroscopy, Fourier Transform Infrared (FTIR) spectrometry, X-ray Diffraction (XRD), XPS, and TEM. The authors also measured hydrogen adsorption at the surface of the plasma-treated samples. While untreated GO samples adsorbed about 1×10^{21} hydrogen molecules per gram, prolonged hydrogen plasma treatment for 1 h resulted in adsorption over 4 times that amount. The results were attributed to the increasing number of carbon vacancies resulting from the hydrogen plasma treatment. Considering Fig. 2, bond scission due to the interaction with energetic photons probably formed the vacancies. High-resolution XPS C1s spectra revealed interesting results. The authors successfully distinguished between C–C (peak at a binding energy of 285.3 eV) and C=C bonds (at 284.5 eV). The short plasma treatment at low power did not cause significant changes, but some samples exhibited a well-pronounced peak at the binding energy of 288.8 eV, which was attributed to either C=O or O=C–OH functional groups. The XPS results correlated with those obtained by FTIR. The authors did not comment on the reasons for the formation of the C=O or O=C–OH functional groups on the surface of samples treated with hydrogen plasma, but considering the properties of hydrogen plasma, as explained in the introduction to this paper, may lead to the conclusion that such groups form upon the defects created in the graphene structure upon exposure to the air. The vacancies and holes were helpful in tuning the catalyst activity of plasma-treated samples.

Ke et al. (2018) used an inductively coupled RF hydrogen plasma at a pressure of 15 Pa, operated in the E mode, to reduce the surface of very thin films composed of GO flakes. The nominal discharge power was 150 W, and the treatment time was 20 min. GO films with a mass of 40 mg were exposed to hydrogen plasma, as shown in Fig. 5. The samples were at floating potential. Optical emission spectroscopy was used to characterize the plasma and revealed significant dissociation of hydrogen molecules (Balmer series predominated the spectrum) as well as an intense Fulcher band. Such plasmas are renowned both as a source of neutral ground-state atoms and of radiation across a broad range of the vacuum ultraviolet and ultraviolet parts of the spectrum (Fantz et al. 2016). AFM analysis revealed that the GO flakes were only up to a few monolayers thick. The authors also demonstrated that plasma treat-

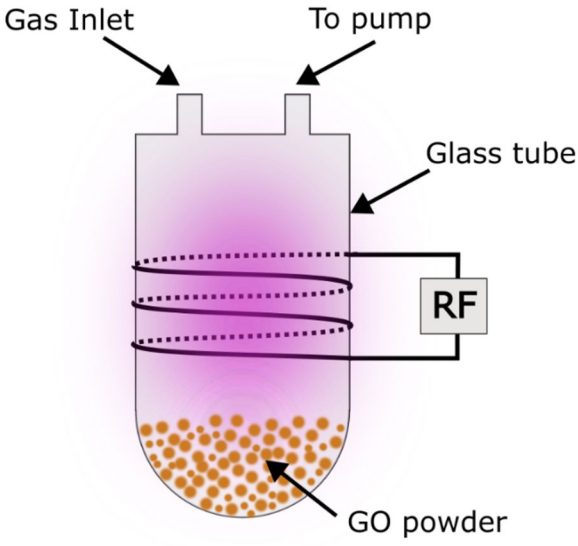

Fig. 5 An illustration of the glass discharge tube for treating GO powder with plasma powered by inductively coupled RF discharge in the E mode, as disclosed by Ke et al. (2018)

ment decreased the average lateral dimension of the GO flakes. The modifications in the structure and composition of treated GO films were probed by XPS and Raman spectroscopy. The XPS showed a significant reduction in the concentration of oxygen groups. Still, the oxygen concentration remained close to about 10 at% even after treating the samples for 20 min. The treatment was found to be useful due to its increased antibacterial activity, attributed to modifications in GO flake size and the formation of nanoneedles. According to the authors, small-sized flakes were particularly destructive for the bacterial membrane.

Torabi et al. (2018) deposited carbon black particles onto GO layers and treated them with hydrogen plasma. The nanocomposites were deposited onto glassy carbon electrodes and evaluated for their charge-storage capabilities. Hydrogen plasma was sustained in a furnace heated to 800 °C, but other details are not disclosed. XPS showed a rather marginal decrease in oxygen-containing functional groups, suggesting that heating to such a high temperature does not cause a significant reduction. However, some authors reported complete deoxidation when GO sheets were heated in a hydrogen atmosphere at equilibrium conditions at such high temperatures (Li et al. 2008). A more trivial explanation of the unexpected result reported by Torabi et al. (2018) may be secondary oxidation and/or adsorption of adventitious carbon. High-resolution C1s spectra revealed that the shake-up peak at approximately 290 eV almost disappeared after the plasma treatment, which may indicate the loss of the original graphene structure. The authors used this composite to test supercapacitors and found a several-fold increase in the specific capacitance after the hydrogen-plasma treatment.

Room temperature reduction of GO was reported by Yang et al. (2018). They used an inductively coupled RF discharge, and plasma was sustained in methane at a pressure of 7 Pa and a discharge power of 100 W. The experimental setup is illustrated in Fig. 6. Inductively coupled plasma is concentrated within the coil connected to an RF generator. The samples are placed a few cm below the plasma source, so the density

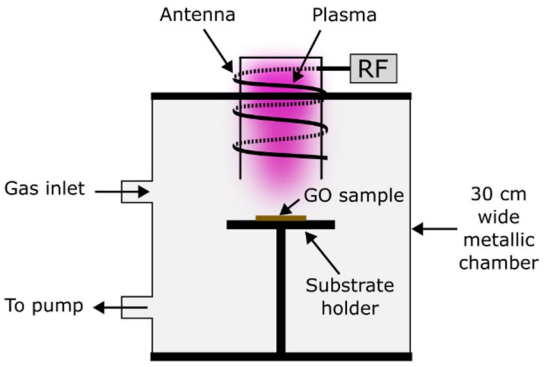

Fig. 6 An illustration of the experimental setup for treating GO samples at room temperature using a remote plasma source, as disclosed in Yang (2018)

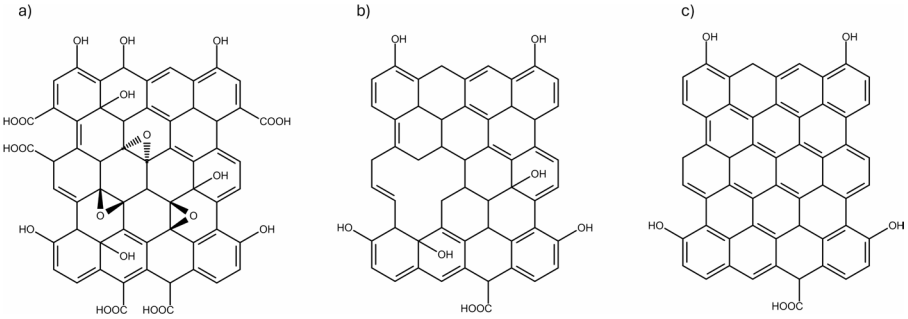

Fig. 7 The effects of plasma rich in both H and C atoms (or CH radicals) on graphene oxide; **a** GO is rich in chemically bonded oxygen; **b** reactive hydrogen species cause reduction, leaving a disordered structure full of vacancies; **c** the vacancies are replaced by carbon atoms due to the interaction with CH_x radicals

of charged particles near the sample surface is low. The flux of energetic photons, however, is large enough to cause bond scission in the upper layer of the GO samples. Such plasma is a source of neutral hydrogen atoms, formed by electron-impact dissociation of CH_4 molecules, and various hydrocarbons, formed by the association of CH_x radicals (Bauer et al. 2005). The radicals will likely stick on the GO surface and form carbon (or hydrogenated carbon) deposits (Honda et al. 2003). The treatment time in methane plasma ranged from 1 to 10 min. XPS showed a gradual decrease in oxygen concentration, which may be attributed to the reduction of GO or the deposition of carbon films from the methane precursor. The oxygen concentration of untreated GO was approximately 38 at%, decreasing to approximately 8 at% after prolonged treatment. The high-resolution C1s peak revealed a rather uniform reduction in the intensity of both C–OH, C=O, and O=C–OH groups. The authors explained the reduction by deoxidation due to interaction with active hydrogen, as well as the repair of vacancies in the reduced GO structure through the incorporation of carbon, sourced from CH_x radicals. In fact, graphene structures free of vacancies are not prone to oxidation by exposure to ambient air. Applying hydrogen plasma with methane addition is a promising approach for producing high-quality porous

films with densely packed graphene flakes. The effects of such a plasma treatment are illustrated in Fig. 7.

Abdelkader-Fernández et al. (2019) treated thin films of graphene oxide with hydrogen plasma sustained by a microwave discharge at a discharge power between 500 and 700 W and a pressure of 50 Pa. The reactor was introduced as "Europlasma Junior Advanced SS", but no details about such a device are accessible. Treatment times ranged from 1 to 10 min. Such a powerful hydrogen plasma is a rich source of H atoms and ions, leading to rapid deoxidation of carbon materials and terminating surface carbon atoms with hydrogen (Liu et al. 2015). The samples were characterized by various techniques. Among them, XPS showed relatively small changes in oxygen concentration. In particular, the untreated samples exhibited an O concentration of 29 at%, whereas plasma treatment under different conditions reduced it to 23 at%. There was no correlation between oxygen concentration and treatment time or discharge power, indicating that the relatively high oxygen concentration in treated samples was due to adventitious carbon rather than incomplete reduction. The temperature-programmed desorption showed significantly different behavior between untreated and plasma-treated samples. Untreated samples exhibited a very intense peak already at the temperature of about 165 °C, which was absent for the hydrogen plasma-treated samples. Still, some carbon dioxide was desorbed even at temperatures above 700 °C, indicating that the GO reduction was not complete. These results are consistent with the composition probed by XPS. Interestingly, the FTIR characterization yielded a completely different result from that of XPS. Primarily, the broad peak corresponding to the OH vibration diminished after the samples were treated with hydrogen plasma. Here, it is worth mentioning that the probing depth of XPS is orders of magnitude smaller than that of FTIR. Some samples were also probed by XPS after heating them at 300 °C. Such samples exhibited a much lower oxygen concentration than the unheated samples. A few samples were also exposed to boiling water before the hydrogen plasma treatment. Interestingly, boiling caused a significant decrease in oxygen concentration. Hydrogen plasma reduction was more efficient for samples boiled in water than for as-synthesized samples. The boiling was performed to purify the samples before the hydrogen-plasma treatment, as the as-synthesized GO samples contained a significant amount of sulfur. XPS survey spectra showed about 3 at% sulfur, and this amount persisted even after plasma treatment. The authors attributed sulfur to sulfonyl and/or sulfonic groups. The rather large amount of oxygen after the hydrogen plasma treatment was attributed to these groups. Since sulfur was removed by prolonged treatment in boiling water, the lower oxygen content in water-treated samples was explained by the absence of the $-SO_2$ or $-SO_2OH$ groups rather than the extensive removal of oxygen bonded directly to carbon.

Fraih et al. (2021) used hydrogen plasma sustained at a pressure of 10,000 Pa to reduce GO samples. The GO suspension was spin-coated onto substrates, but further details are not provided. The as-deposited film thickness was about 25 nm. Raman spectra showed a decrease in the I_D/I_G ratio with increasing hydrogen-plasma treatment time. The ratio for untreated GO was about 1, dropping to 0.6 after 10 min of treatment time. The electrical resistance dropped from 12.1 to 0.34 MΩ.

Magureanu et al. (2021) deposited GO films on an unspecified substrate and exposed them to plasma sustained by a DC glow discharge. The discharge was sustained in hollow-cathode mode, with a discharge voltage ranging from 2 to 5 kV. Such a discharge creates plasma with a moderate ion density and moderate density of H atoms (Méndez et al. 2006). The hydrogen pressures ranged from 20 to 400 Pa. The samples were treated either in the negative glow or the positive column. Somewhat unexpectedly, the spectra of the positive column as probed by optical emission spectroscopy were free from the Balmer atomic lines, and only the Fulcher band was detected in the range of wavelengths between 425 and 675 nm, together with a strong continuum arising from the dissociative relaxation of highly excited hydrogen molecules. The gas temperature depended on the discharge power and ranged from 350 to 500 K. HR XPS C1s spectra revealed a significant reduction in the ~286–288 eV spectral region, which covers the oxygen-related bonds. However, numerical values regarding oxygen concentration were not provided. The authors performed DFT calculations and modelled the reduction by forming hydroxyl groups as the first step, followed by creating a water molecule (which desorbs upon vacuum conditions), and terminating the dangling bond with a hydrogen atom.

Zhang et al. (2022) deposited thin films of GO on Teflon foils. The samples were then peeled off and treated with hydrogen plasma at a pressure of 500 Pa. The type of discharge was not explicitly stated, but the photo of a simple plasma system indicates inductive coupling of a low-power RF generator, similar to the reactor illustrated in Fig. 5. The treatment times ranged from 0 to 120 s, and the discharge power varied between 10 and 50 W. FTIR analysis revealed a gradual decrease in the concentration of oxygen-containing functional groups, particularly a reduction in the broad range around 3,300 cm^{-1}, indicating a preferential removal of the OH group. The quantitative estimate of the reduction efficiency was based on Energy-Dispersive X-ray Spectroscopy (EDX) results. Untreated samples exhibited 36 wt% of oxygen, dropping to 33 wt% after 40 s and 28 wt% after 60 s of plasma treatment. XPS was available only for the untreated sample, and a high concentration of C–C–O and/or C–O–C groups was reported.

Hamzaj et al. (2024) treated GO samples with hydrogen plasma sustained by RF ICP discharge in the E mode. The hydrogen pressure was 32 Pa, and the forward power was 100 W. The samples were placed in the early afterglow of hydrogen plasma and treated for varying periods, ranging from 10 to 240 s. Pulsed treatment with 10-s pulses was used to prevent overheating caused by exothermic surface reactions. Untreated GO samples exhibited wrinkles that persisted even after plasma treatment. XPS showed a significant decrease in the concentration of oxygen functional groups, particularly the peak at approximately 287 eV, which was found to be a convolution of the C–O and C=O bonds. The authors used reduced GO samples as an NH_3 sensor device, showing good reversibility and lower sensitivity with more prolonged plasma exposure, and vice versa with shorter plasma exposure.

Eda et al. (2013) reported self-limiting reduction of the uppermost layers of GO upon treatment with hydrogen plasma. Using the drop-casting method, a colloidal GO suspension was deposited on a quartz substrate. Hydrogen plasma was sustained at the discharge power as low as 2 W and a pressure of 130 Pa. The treatment time varied up to 1200 s. The original sheet resistance of such films was 10^{11} Ω/sq, drop-

ping to about 10^7 Ω/sq after 10 min of plasma treatment. This paper thus reports a significant increase in the electrical conductivity upon the transformation of GO to almost oxygen-free graphene. Unfortunately, the details about the sample composition were not provided. The plasma treatment was found useful for field-effect transistors.

Hazarika et al. (2025) treated self-standing GO films in hydrogen plasma sustained by a DC glow discharge at a pressure of 20 Pa for 30 min at 6 W discharge power. The plasma reactor is illustrated in Fig. 8. It is made from stainless steel. The feedthroughs separated the electrodes from the grounded chamber. The dimensions of both electrodes were the same. The discharge voltage was about 600 V, and the discharge was in the normal glow regime. In such a discharge, the major voltage drop is in the sheath next to the cathode, and the anode self-biases near the floating potential. The samples were placed on the cathode, where they were exposed to energetic hydrogen ions, leading to significant etching. The etching caused nanospikes on the originally rather smooth GO surface, as evidenced from AFM images. The electron temperature in the positive column was 1.4 eV. The discharge chamber was metallic, so plasma with such a low electron temperature should not be a significant source of H atoms (Kroon 1997). Furthermore, H atoms are lost on the surfaces because of the rather large coefficient for heterogeneous recombination of H atoms on stainless steel (Mozetic and Zalar 1999). The low H-atom density is reflected in the relatively low reduction efficiency, as indicated by the EDX spectra, which show a decrease in oxygen concentration from 35 at% to 28 at%. XPS showed the oxygen concentration of 32 at% and 26 at%, respectively. The authors proposed a mechanism for reducing GO upon treatment with hydrogen plasma. The C–OH group was supposed to interact with 2 hydrogen atoms, substituting the OH surface group with a hydrogen group

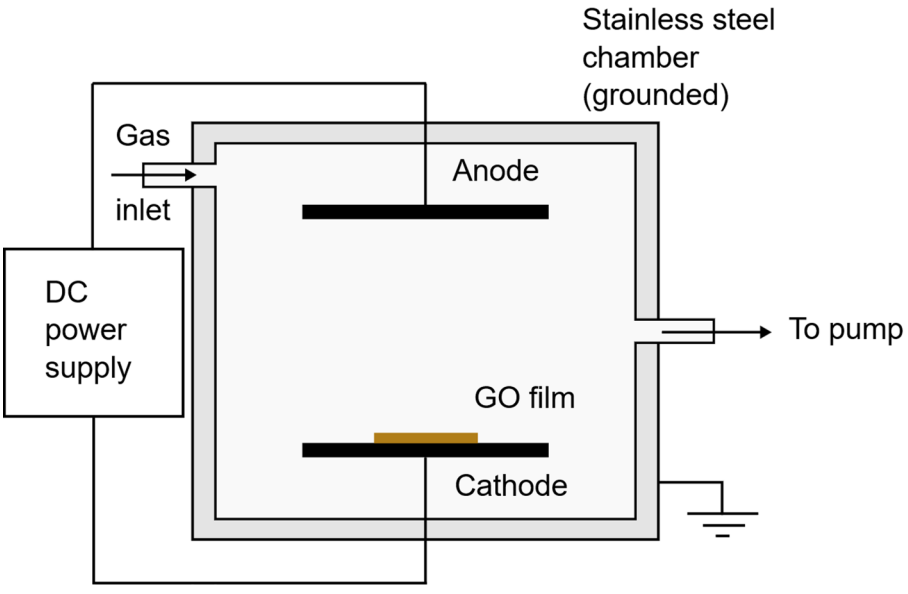

Fig. 8 Illustration of the plasma reactor used by Hazarika et al. (2025)

and forming a water molecule, which desorbed from the surface under low-pressure conditions. This model agrees with the early report of Magureanu et al. (2021). The epoxy group also reacted with 2 hydrogen atoms, forming a water molecule. On the other hand, the C=O group was proposed to be reduced to a hydroxyl group, whereas the O=C–OH group will be destroyed by releasing a CO_2 molecule and a H_2O molecule. As oxygen functional groups are removed, GO begins to reestablish its sp^2 carbon network. High-resolution C1s peaks revealed that the concentration of O=C–OH groups dropped below the XPS detection limit after the hydrogen plasma treatment. In contrast, the concentration of C=O groups increased after hydrogen plasma treatment, from the original 7at.% to 15 at%. The authors have not commented on this rather unexpected result, but it may be due to secondary oxidation upon exposure of plasma-treated samples to air. In fact, the absorption of VUV photons and bombardment by positively charged hydrogen ions (the samples were on the cathode, with a discharge voltage of 600 V) should cause significant radiation damage in the GO film's surface layer. The electrical resistance of self-standing films decreased by a factor of 4 after hydrogen plasma treatment.

Kosaentor et al. (2024) treated self-standing GO films of densely packed GO sheets with energetic ions using a home-made discharge tube, which is shown in Fig. 9. The source of ions was a low-pressure plasma sustained by an RF discharge in either argon or hydrogen. The gas pressure in the plasma source was about 0.07 Pa. The thickness of the GO films placed onto the biased electrode was about 2 μm. The discharge power was 100 W, and a negative voltage of 5 kV was applied to the sample holder as shown in Fig. 9. The negative voltage was supplied in 10-μs pulses at a frequency of 100 Hz. Such a pulsed treatment prevented excessive thermal loads. The treatment times ranged from 2 to 8 min. The kinetic energy of the positively charged ions was large enough to penetrate rather deeply inside the GO films. The authors

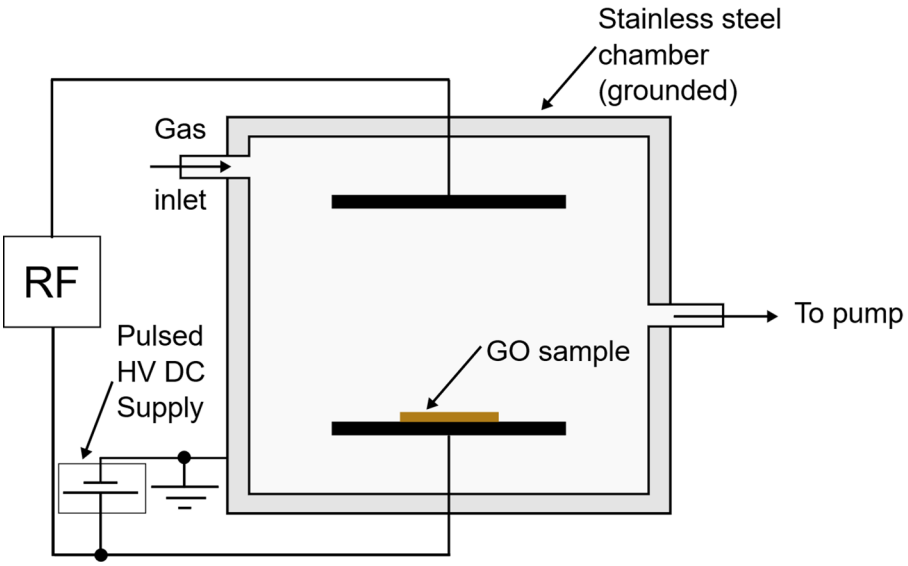

Fig. 9 Illustration of the discharge configuration used by Kosaentor et al. (2024)

reported a penetration depth of H^+ ions close to 100 nm. The XPS analysis revealed a moderate decrease in oxygen concentration after the plasma treatment. Treatment with hydrogen plasma for 8 min resulted in a threefold decrease in the concentration of the C–O group and a significant increase in the concentration of C=C/C–C bond. Interestingly, the concentration of the C=O group remained fairly unchanged at about 9 at%, which is consistent with previously reviewed papers that reported preferential removal of the hydroxyl group. The concentration of O=C–OH groups increased significantly for all plasma treatments. The concentration of this group on the untreated GO films was approximately 4 at%, and the concentrations after 2, 4, and 8 min of H_2 plasma treatment were 8, 9, and 7 at%, respectively. The sheet resistance was about 1.4 MΩ/sq for the untreated sample and dropped to 0.6, 0.7, and 0.5 MΩ/sq, respectively. The decrease is rather marginal compared with Fraih et al. (2021), let alone Eda et al. (2013). The relatively minor increase in conductivity may be attributed to radiation damage resulting from treatment with energetic ions. Irradiation with energetic hydrogen ions causes disorder in carbon bonds, stimulates the formation of a diamond-like carbon structure, and leads to the creation of glassy carbon nanoparticles (Liu et al. 2021). Hydrogen remains trapped (chemically bonded) in the carbon materials after ion implantation (Begrambekov et al. 2009). All these effects are detrimental to the electrical conductivity. The effects of ion bombardment are illustrated in Fig. 10.

2.2 Atmospheric-pressure plasma treatment

One of the first reports about applying atmospheric-pressure hydrogen plasma for GO reduction was reported by Bodik et al. (2017). They prepared a thin GO film by Langmuir-Schaeffer deposition. Hydrogen plasma was sustained in a chamber at atmospheric pressure by a dielectric coplanar surface barrier discharge (DCSBD). Such plasma is sustained in the form of streamers, which propagate close to the surface of the dielectric plate with embedded electrodes. The average electron temperature in a streamer was estimated to be 11,000 K, and its density was about 10^{20} m^{-3}. The density was significantly lower in the volume away from the streamers due to the loss of charged particles in the gas phase. The neutral gas temperature was close to the room temperature. The surface power density, normalized per electrode area, was close to 2 W/cm². The sample distance from the dielectric plate with embedded electrodes was 0.15 mm. The treatment times ranged from 1 to 5 s. The distance was

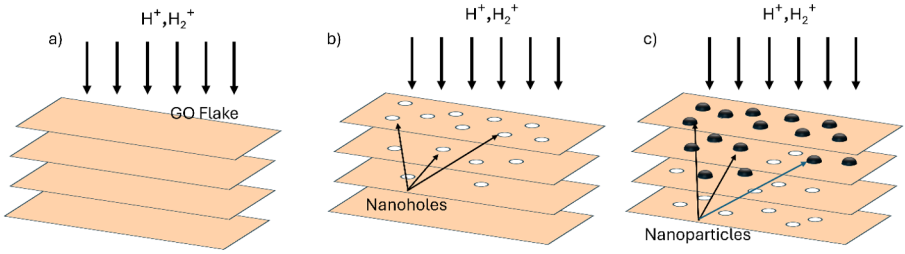

Fig. 10 Schematic of the treatment with energetic ions (**a**), and structural modifications of graphite-like materials upon irradiation with hydrogen ions (**b**), and creation of carbon nanoparticles (**c**)

altered in another set of experiments, while the treatment time remained constant at 5 s. The samples were probed by XPS. The reduction was incomplete, despite using a rather powerful discharge to sustain hydrogen plasma. The authors, however, reported even better results when using methane plasma. The better performance of methane plasma was attributed to the higher ionization energy of hydrogen molecules compared to that of methane. Another possible explanation could be deduced from experiments reported by Yang et al. (2018): deposition of carbon material on the GO flakes by sticking of CH_x radicals. The effects observed by Bodik et al. (2017) may be similar to those illustrated in Fig. 7.

Atmospheric pressure plasma was also used by Gemeiner et al. (2020) to reduce GO samples. The average thickness of the GO layers was 50 nm, but it was laterally highly inhomogeneous, as thicknesses ranging from 20 to 160 nm were reported. The authors utilized the DSCBD for sustaining hydrogen plasma, and the reported power density was 100 W/cm³. HR XPS C1s spectra revealed a significant decrease in the concentration of oxygen functional groups, particularly the group that peaked at (by authors unspecified peak) at binding energy of 288 eV, which should correspond to either C-O-C or C-OH. The best results were obtained after a plasma treatment time of 8 s, and the authors also reported a transformation of sp^3 carbon to sp^2. The treatment was useful for the synthesis of dye-sensitized solar cells.

Similar GO deposits were also used by Homola et al. (2018). Apart from a significant reduction of the GO due to hydrogen plasma treatment, the authors also reported decreased deposit thickness, which they attributed to etching. After treating the samples with hydrogen plasma for 10 s, the oxygen concentration dropped to about 11 at%. However, a significant concentration of silicon was also reported in XPS survey spectra. The authors found the surface kinetics difficult to explain because of the large gradients in the concentration of reactive plasma species at atmospheric pressure. The authors found long-lived radicals capable of modifying GO flakes at the edges, ripples, or other defects.

The specifics of plasma treatments at atmospheric pressure using the coplanar surface barrier discharge are illustrated in Fig. 11. Electrodes are embedded in an alumina plate and powered by a high-impedance low-frequency (10–30 kHz) RF generator. Streamers occur in the gas phase, as shown in Fig. 11, because alumina is a better insulator than the working gas at atmospheric pressure. The distance between the neighboring electrodes in the alumina plate is about 1 mm. Such a configuration enables a rather stable discharge with several streamers per RF period. The carbon samples are placed close to the alumina plate, with a distance of less than 1 mm, or even as close as 0.1 mm. None of the authors reported shortcuts, i.e., appearance of streamers on the shortest path, i.e., from an electrode to the graphene sample and then

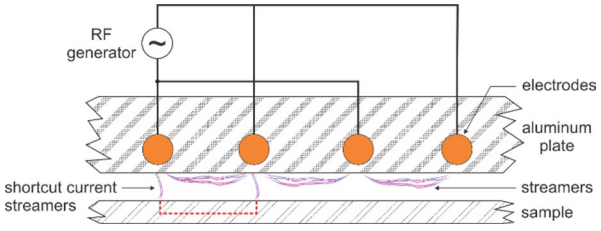

Fig. 11 Illustration of the coplanar surface barrier discharge for treatment of GO films. A self-standing film is shown for simplicity, but it is likely attached to a rigid holder in practical cases to maintain a constant distance from the alumina plate. Not to scale

from the graphene sample to the opposite electrode, as marked with "shortcut current streamers" and dashed red lines in Fig. 11.

2.3 Summary

The results reported by different authors are summarized in Table 1. Many authors reported the gas pressure, the type of discharge used for sustaining hydrogen plasma, and the discharge power. Most authors varied the treatment time. The reduction is the most significant effect of hydrogen plasma treatment; therefore, we included a column showing the initial and final oxygen concentrations, as measured by XPS, in Table 1. Some authors used EDX, and we added these values to the same column, although XPS and EDX are different techniques, so the concentration of elements often varies significantly due to the different probing depths of XPS and EDX. Different authors also employed various complementary techniques for material characterization; however, these are not included in Table 1 because they are statistically insignificant and would make the table difficult to read.

Table 1 Summary of research papers on hydrogen plasma reduction of graphene oxide

Author	Gas type, pressure	Power [W]	t_{treat}	Initial O conc. [%]	Final O conc. [%]	Δ O conc. [abs. %]	T_{MAX} [°C]
Hafiz et al. (2014)	H_2 50–80	10	20–40 s	55	11	44	27
Singh et al. (2014)	H_2 at 50 Pa	15–30	10–300 s	33	14	19	50–120
Jesuraj et al. (2018)	H_2 at 40 Pa	15	1 min	36.7	26.21	10.5	NA
Banerjee et al. (2018)	H_2 at 1 bar	20–60	30 min	NA	NA	NA	RT
Primo et al. (2018)	H_2 at 10 Pa	0.4–2	15–60 min	8*	16	+8	NA
Ke et al. (2018)	H_2 at 15 Pa	150	20 min	NA	NA	NA	NA
Torabi et al. (2018)	H_2/Ar 3:7	NA	1 h	38.2	21.1	17.1	800
Yang et al. (2018)	CH_4/Ar at 7 Pa	100	1–10 min	31	8	23	RT
Abdelkader-Fernández et al. (2019)	H_2 at 50 Pa	500/ 700	1/5/10 min	29.1	25.5	3.6	NA
Fraih et al. (2021)	H_2 at 10 kPa	3 W/cm^2	2/4/6/8/10 min	NA	NA	NA	NA
Magureanu et al. (2021)	H_2 at 200–400 Pa	0.41–1.36	NA	NA	NA	NA	350–500 K
Zhang et al. (2022)	H_2 at 500 Pa	10/30/ 50	10–120 s	36.6	28.5	8.1	NA
Hamzaj et al. (2024)	H_2 at 32 Pa	100	10–240 s	NA	NA	NA	RT
Eda et al. (2013)	H_2 at 130 Pa	2	0–1200 s	NA	NA	NA	NA
Hazarika et al. (2025)	H_2 at 20 Pa	6	30 min	31.85	25.55	6.30	NA
Kosaentor et al. (2024)	Ar or H_2 at 0.07 Pa	100	2/4/8 min	32.29	20.42	11.8	NA
Bodik et al. 2017)	H_2 or CH_4 at 1 bar	100	1–5 s	30.5	5.8	24	RT
Gemeiner et al. (2020)	H_2 at 1 bar	100 W/cm^3	8 s	NA	NA	NA	RT
Homola et al. (2018)	H_2 at 1 bar	240	8 s	27.3	11.1	16.2	RT

*After prior hydrothermal reduction

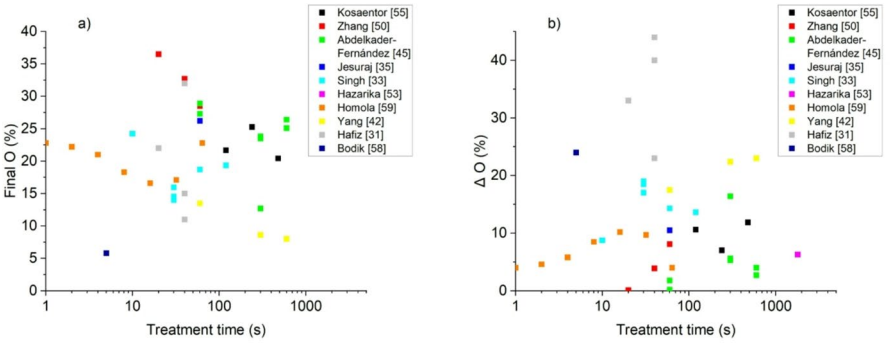

Fig. 12 **a** Final concentration of oxygen as reported from XPS or EDX spectra versus the treatment time; **b** difference in oxygen concentration for plasma-treated and untreated samples versus the treatment time. The ΔO is zero for untreated samples

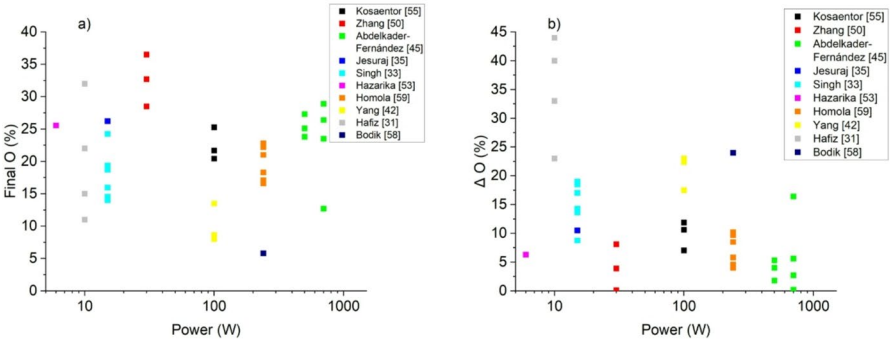

Fig. 13 **a** Final concentration of oxygen as reported from XPS or EDX spectra versus the discharge power; **b** difference in oxygen concentration for plasma-treated and untreated samples versus the discharge power. The ΔO is zero for untreated samples

3 Correlations

Table 1 reveals that different authors employed various experimental conditions, making direct comparison of the results difficult. Still, we performed a meta-analysis, and the correlations between the observed results and the treatment parameters are illustrated in Figs. 12, 13, 14, 15 and 16. We plotted the following correlations:

- The concentration of oxygen on the treated samples versus the plasma treatment time (Fig. 12a),
- The difference in concentration of oxygen after and before the plasma treatment versus the treatment time (Fig. 12b),
- The concentration of oxygen versus the discharge power (Fig. 13a),
- The difference in concentration of oxygen after and before the plasma treatment versus the discharge power (Fig. 13b),
- The oxygen concentration versus the product of the discharge power and the

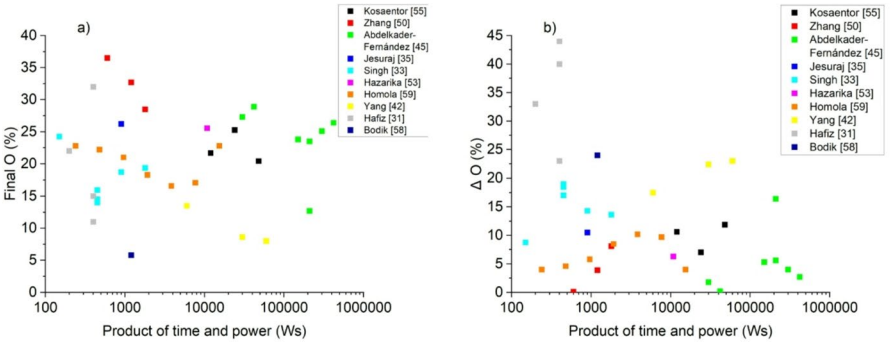

Fig. 14 Concentration of oxygen **a** and the difference in oxygen concentration **b** versus the product of the treatment time and the discharge power. The ΔO is zero for untreated samples

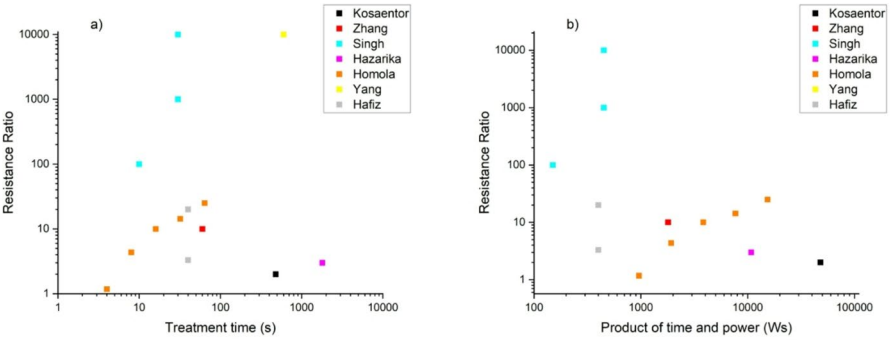

Fig. 15 The ratio of electrical resistance before and after plasma treatment versus the treatment time (**a**) and versus the product of the treatment time and the discharge power (**b**)

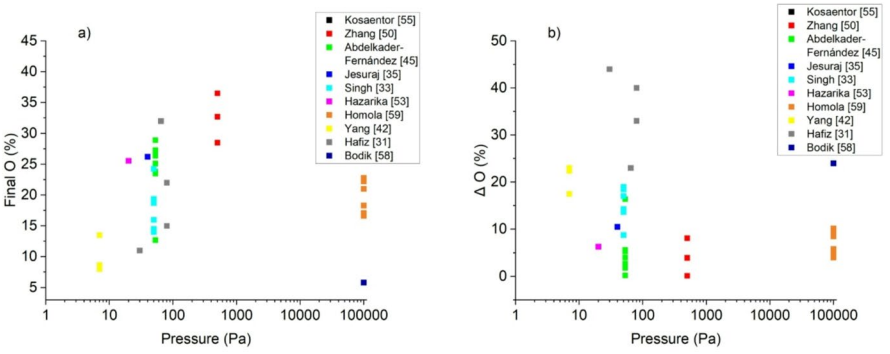

Fig. 16 **a** Concentration of oxygen versus the pressure; **b** difference in oxygen concentration versus the pressure. The ΔO is zero for untreated samples

treatment time (Fig. 14),
- The change in the electrical resistance (Fig. 15), and.
- The concentration of oxygen versus the gas pressure in the plasma reactor (Fig. 16).

Figure 12a shows the final oxygen concentration, as reported from XPS or EDX spectra, plotted against treatment time. The original oxygen concentration varied, but the average was about 40 at%. One can observe that all authors reported a decrease in oxygen concentration as a result of hydrogen plasma treatment. Some authors, such as Abdelkader-Fernández et al. (2019) and Hazarika et al. (2025), reported a marginal decrease, whereas others found the final concentration to be as low as approximately 10 at%. Most authors reported a final oxygen concentration of approximately 20 at%. Interestingly, no author reported an oxygen concentration below 5 at%. This observation may suggest an incomplete reduction of the GO samples; however, a more feasible explanation is secondary oxidation due to the exposure of the samples to air before XPS or EDX characterization, or simply because of the adsorption of organic gaseous impurities on plasma-treated samples, since these impurities usually contain a significant concentration of oxygen (Grey et al. 2025). Many authors reported the formation of dangling bonds as a result of hydrogen plasma treatment (Li et al. 2016; Zhang et al. 2022; Kosaentor et al. 2024), and these bonds are likely to be occupied with oxygen after exposure to air. Interestingly, Fig. 12a reveals no correlation between the final oxygen concentration and the treatment time, indicating that the latter is not the parameter governing the reduction of graphene oxide.

As already mentioned, the original oxygen concentration varied; therefore, a more appropriate presentation of the results is the difference in oxygen concentration between plasma-treated and untreated samples. This correlation is plotted in Fig. 12b. On average, the concentration difference is approximately 10%, which is relatively small. Again, there is no correlation between the drop in the oxygen concentration and the treatment time.

The flux of plasma species on treated materials should increase with increasing discharge power. The concentration of oxygen in the samples after treating them with hydrogen plasma is plotted in Fig. 13. Figure 13a represents the final concentration of oxygen vs. the discharge power, and Fig. 13b is the oxygen concentration difference versus the discharge power. There is hardly any correlation in Fig. 13a.

Surprisingly, Fig. 13b suggests a decrease in reduction efficiency with increasing discharge power. The measured points in Fig. 13b are scattered, but it appears that lower discharge powers enable a larger drop in oxygen concentration on the surface of plasma-treated GO samples. It is difficult to explain the paradox, but one feasible explanation is to account for the damage caused by treatment at a higher discharge power. As already mentioned, hydrogen plasma is a source of chemically reactive particles (neutral hydrogen atoms in particular) and VUV/UV radiation. The reactive particles interact with oxygen bonded to the graphene sheets, forming a water molecule. On the other hand, radiation causes bond scission, which is not beneficial. The radiation thus causes defects in the reduced GO structure, and these defects may be prone to chemically bond to oxygen upon exposure of the plasma-treated samples to air prior to XPS or other characterization. Furthermore, the defects caused by exces-

sive VUV/UV radiation are likely to form bonds with the adventitious carbon. The net effect would be a higher oxygen concentration in the longer treated samples. The effect is illustrated in Fig. 17, which shows the proposed effect of hydrogen plasma treatment on the GO lattice/structure.

A layer of adventitious carbon forms on virtually all materials exposed to the air. In particular, ambient air contains minute amounts of volatile organic compounds. The types of compounds vary, and so do their concentrations. They include benzene, chloroform, styrene, formaldehyde, freon, and short-chain hydrocarbons (Grey et al. 2025). Once an impurity-free surface of a solid material is exposed to air, volatile organic compounds in the air adhere to the surface due to weak van der Waals forces. The amount of adsorbed adventitious carbon obviously depends on its concentration in the air and exposure time. The layer is rarely thick because the attractive force decreases with increasing distance from the surface. It is usually a few nm. Formation of thicker films is prevented by the desorption, which increases with the vapor saturated pressure.

We anticipate that the plasma species dose will scale positively with both discharge power and treatment duration. Figure 14a represents the final oxygen concentration as a function of the product of discharge power and treatment time, while Fig. 14b shows the oxygen concentration difference. According to Fig. 17, one would expect a large concentration of oxygen at larger products of the discharge power and time. However, the data presented in Fig. 14a do not support such speculation. Nevertheless, a trend is rather evident in Fig. 14b. An obvious conclusion is that the radiation damage depends on the discharge power and the dose of reactive hydrogen species.

The reduction rate and the concentration of radiation-induced defects should govern the electrical conductivity of reduced GO samples. Figure 15a and b represent the change in either conductivity, sheet resistance, or resistivity ratio (denoted s resistance ratio) reported by different authors. Interestingly, the resistance ratio is higher for small values of the product of the treatment time and the discharge power. Thus, the diagrams presented in Fig. 15 support the hypothesis, which is illustrated in Fig. 17.

Many authors reported oxygen concentration obtained at different pressures. Figure 16 summarizes the results. Again, there is no correlation between oxygen concentration and gas pressure; however, atmospheric-pressure plasma appears to enable better reduction than low-pressure plasma, because the lowest oxygen concentration

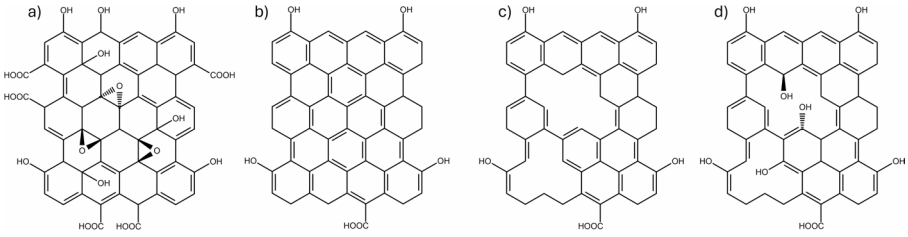

Fig. 17 The proposed effect of hydrogen plasma treatment. **a** GO before the treatment contains lots of oxygen; **b** treatment at a low discharge power causes reduction and thus formation of graphene; **c** treatment at high power causes reduction, and also radiation damage; **d** the defects are occupied by oxygen after exposure to the air

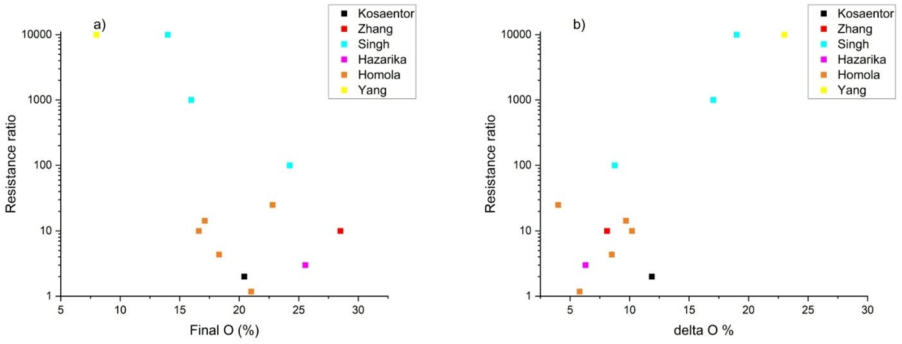

Fig. 18 The resistance ratio (i.e., the reported sheet resistance of untreated samples divided by the sheet resistance after hydrogen plasma treatment) as a function of the oxygen concentration after the plasma treatment (**a**), and as a function of the difference in oxygen concentration (**b**)

after plasma treatment at atmospheric pressure is only about 5%. Still, the number of experiments at atmospheric pressure is insufficient to bring decisive conclusions.

According to the above discussion, electrical conductivity should increase as the oxygen concentration decreases. Figure 118 illustrates the correlation between the resistance ratio and oxygen concentration. There is insufficient data to draw a firm conclusion, but the trend presented in Fig. 18b supports the hypothesis, i.e., a larger change in oxygen concentration will result in a larger change in conductivity.

Finally, it is worth emphasizing that the surface modifications depend on the fluxes of reactive hydrogen species and treatment time (or the dose, which is the product of these variables as long as the flux remains constant). No reviewed paper mentioned the fluxes, so it is impossible to draw any conclusive remark on the exact kinetics of the interaction between hydrogen plasma and graphene oxide samples.

4 Conclusions and roadmap

The analysis of available data on the reduction of graphene oxide flakes by exposure to hydrogen plasma reveals some interesting features. Almost all authors reported a reduction of oxygen concentration in GO films and structures, as expected. Rather unexpected is the observation that longer treatment times do not result in lower oxygen concentrations, and higher discharge powers yield worse results than lower discharge powers. These two paradoxes were explained by taking into account the peculiarities of the experimental systems used by different authors. Most likely, there are two competing effects of the hydrogen plasma treatment: the reduction and the radiation damage. While oxygen concentration can be taken as indication of reduction process (chemical and physical), this parameter can not fully uncover the radiation damage by plasma particles/species. Therefore, we compared the published results also using resistance ratio change, since such damage destruction will be reflected in a change in the structure of the material and thus its electrical properties. The reduction in the oxygen concentration occurs predominantly through the exposure of the GO samples to hydrogen atoms. The atoms chemically interact with the GO surface,

thus causing a reduction in oxygen concentration. The detailed investigation of the reviewed papers indicates that the hydroxyl groups on the GO samples are more likely to be reduced than some other groups. The reduction should be accomplished already at a reasonably low dose of H atoms. The quantification (i.e., plotting a correlation between the H-atom dose and the concentration of remaining oxygen) is yet to be performed and represents a major scientific challenge. Obviously, the quantification needs information about the flux of H atoms on the GO samples, but none of the reviewed articles provided any numerical value.

While H atoms are beneficial because they are supposed to cause a significant reduction of graphene oxide, the radiation arising from hydrogen plasma most likely has a negative effect. The results reported by different authors indicate that VUV and perhaps also UV radiation cause radiation damage to the graphene sheets, resulting in numerous defects. The defects are likely to interact with oxygen upon exposure to the air and cause secondary oxidation. If this is the major reason for the incomplete reduction of GO samples, a straightforward experiment should be performed in the fore-chamber of an XPS instrument, allowing the samples to be analyzed without exposure to air. This is another scientific challenge.

An alternative mechanism that may cause a rather large amount of oxygen on the surface of plasma-treated samples is the adsorption of organic impurities from the air. This effect should be suppressed by the installation of the sample into the XPS chamber immediately after the plasma treatment, or, preferably, by treatment in the XPS fore-chamber. Unfortunately, the reviewed articles did not report the time between plasma treatment and the transport of treated samples into the XPS (or SEM) chamber, so we could not establish a correlation.

An interesting approach with potential for industrial applications is admixing hydrocarbons with hydrogen plasma, or post-treating hydrogen plasma-treated graphene oxide with plasma sustained in methane or another hydrocarbon gas. A couple of articles have emphasized the beneficial effect, which is attributed to the binding of carbon from CH_x radicals to defects in the graphene structure after treatment with hydrogen plasma. A scientific challenge is to determine the correlation between the dose of CH_x radicals and the surface finish, particularly the concentration of oxygen, after exposing such samples to air. A technologically more significant challenge is to plot the correlation between the peculiarities of the plasma sustained in hydrocarbon gases and electrical conductivity. The flux of CH_x radicals is not trivial to measure, so any estimation would do.

With all the experiments suggested above, the hydrogen plasma treatment of graphene oxide represents an interesting method for preparing graphene-like structures for use in electrochemical devices, including batteries and supercapacitors. The GO flakes are relatively easy to synthesize in macroscopic quantities and can be used for the synthesis of paper-like macroscopic structures with a very large surface-to-mass ratio and reasonably high electrical conductivity. These two properties are essential for example for developing fast-response supercapacitors, which offer advantages over Li- or Na-ion batteries.

Acknowledgements This research was funded by the Slovenian Research and Innovation Agency, research project number L2-60139 (Innovative plasma-assisted synthesis of the next-generation high power density

supercapacitor electrodes using graphene oxide feedstock), and research core funding number P2-0082 (Thin film structures and plasma-surface engineering).
František Zelenák is a Brno Ph.D. talent scholarship holder – funded by the Brno city municipality. This work was supported by the project LM2023039 funded by the Ministry of Education, Youth and Sports of the Czech Republic.

Author contributions Conceptualization, F.Z. and M.M.; resources, A.V. and M.M.; data curation, M.M. and F.Z.; writing—original draft preparation, F.Z. and M.M.; writing—review and editing, M.M., A.V., R.Z., GP and R.K.; visualization, F.Z., G.P. and R.Z.; supervision, R.K, D.K and M.M.; project administration, D.K., A.V. and M.M.; funding acquisition, D.K., A.V. and M.M. All authors have read and agreed to the published version of the manuscript.

Funding Open access publishing supported by the institutions participating in the CzechELib Transformative Agreement.

Declarations

Conflict of interest On behalf of all authors, the corresponding author states that there is no conflict of interest.

References

V.K. Abdelkader-Fernández, M. Melguizo, M. Domingo-García et al., Hydrogen cold plasma for the effective reduction of graphene oxide. Appl. Surf. Sci. **464**, 673–681 (2019). https://doi.org/10.1016/j.apsusc.2018.09.121

M. Acik, G. Lee, C. Mattevi et al., The role of oxygen during thermal reduction of graphene oxide studied by infrared absorption spectroscopy. J. Phys. Chem. C **115**, 19761–19781 (2011). https://doi.org/10.1021/jp2052618

H. Akbi, S. Rafai, A. Mekki et al., Kinetic investigation of the multi-step thermal decomposition of graphene oxide paper. J. Therm. Anal. Calorim. **148**, 3487–3503 (2023). https://doi.org/10.1007/s10973-023-11948-1

I. Banerjee, S.K. Mahapatra, C. Pal et al., Effect of plasma power on reduction of printable graphene oxide thin films on flexible substrates. Mater. Res. Express. **5** (2018). https://doi.org/10.1088/2053-1591/aac04e

M. Bauer, T. Schwarz-Selinger, H. Kang, von A. Keudell, Control of the plasma chemistry of a pulsed inductively coupled methane plasma. Plasma Sources Sci. Technol. **14**, 543 (2005). https://doi.org/10.1088/0963-0252/14/3/017

H.A. Becerril, J. Mao, Z. Liu et al., Evaluation of solution-processed reduced graphene oxide films as transparent conductors. ACS Nano. **2**, 463–470 (2008). https://doi.org/10.1021/nn700375n

L.B. Begrambekov, A.S. Kuznetsov, P.A. Shigin, Hydrogen trapping in depositing carbon films. J. Nucl. Mater. **390–391**, 685–688 (2009). https://doi.org/https://doi.org/ https://doi.org/10.1016/j.jnucmat.2009.01.189

M. Bodik, A. Zahoranova, M. Micusik et al., Fast low-temperature plasma reduction of monolayer graphene oxide at atmospheric pressure. Nanotechnology. **28** (2017). https://doi.org/10.1088/1361-6528/aa60ef

G. Chen, L.L. Raja, Fluid modeling of electron heating in low-pressure, high-frequency capacitively coupled plasma discharges. J. Appl. Phys. **96**, 6073–6081 (2004). https://doi.org/10.1063/1.1818354

A. Drenik, A. Vesel, A. Kreter, M. Mozetič, Recombination of hydrogen atoms on fine-grain graphite. Appl. Surf. Sci. **257**, 5820–5825 (2011). https://doi.org/10.1016/j.apsusc.2011.01.111

D.J. Economou, Modeling and simulation of fast neutral beam sources for materials processing. Plasma Process. Polym. **6**, 308–319 (2009). https://doi.org/10.1002/ppap.200900005

G. Eda, A. Nathan, P. Wöbkenberg et al., Graphene oxide gate dielectric for graphene-based monolithic field effect transistors. Appl. Phys. Lett. **102** (2013). https://doi.org/10.1063/1.4799970

U. Fantz, S. Briefi, D. Rauner, D. Wünderlich, Quantification of the VUV radiation in low pressure hydrogen and nitrogen plasmas. Plasma Sources Sci. Technol. **25** (2016). https://doi.org/10.1088/0963-0252/25/4/045006

A.J. Fraih, H.M. Mutlaq, Controlled reduction of graphene oxide via hydrogen plasma for tuning sensitivity and recovery time of rGo based oxygen gas sensor. EPJ Appl. Phys. **95**, 2–6 (2021). https://doi.org/10.1051/epjap/2021210108

B.L. French, J.J. Wang, M.Y. Zhu, B.C. Holloway, Evolution of structure and morphology during plasma-enhanced chemical vapor deposition of carbon nanosheets. Thin Solid Films. **494**, 105–109 (2006). https://doi.org/10.1016/j.tsf.2005.07.155

E.M. Gallo, B.I. Willner, J. Hwang et al., Chemical vapor deposition of graphene on copper at reduced temperatures, in Carbon Nanotubes, Graphene, and Associated Devices V, ed. by D. Pribat, Y.-H. Lee, M. Razeghi (SPIE, 2012), p. 846203

P. Gemeiner, T. Homola, M. Hatala, M. Mikula, Low-temperature hydrogen plasma reduction of graphene oxide counter electrodes for printed dye-sensitized solar cells. NANOCON Conf. Proc. Int. Conf. Nanomater 210–214 (2020). https://doi.org/10.37904/nanocon.2019.8700

L.H. Grey, H. Nie, M.C. Biesinger, Defining the nature of adventitious carbon and improving its merit as a charge correction reference for XPS. Appl. Surf. Sci. **653**, 159319 (2025). https://doi.org/10.1016/j.apsusc.2024.159319

B. Gurzęda, N. Boulanger, M.R.V. Jørgensen et al., Graphite oxide by chlorate route oxidation without HNO3: Does acid matter? Carbon N Y 221 (2024) https://doi.org/10.1016/j.carbon.2024.118899

T. Hazarika, R. Ghosh, G. Saikia et al., Controlled reduction of graphene oxide (GO) film using low-density glow discharge hydrogen plasma. IEEE Trans. Plasma Sci. PP. 1–12 (2025). https://doi.org/10.1109/TPS.2025.3549139

U. Hofmann, Über Graphitsäure und die bei ihrer Zersetzung entstehenden Kohlenstoffarten (Ber Dtsch Chem Ges) (1928)

T. Homola, J. Pospíšil, R. Krumpolec et al., Atmospheric dry hydrogen plasma reduction of inkjet-printed flexible graphene oxide electrodes. ChemSusChem. **11**, 941–947 (2018). https://doi.org/10.1002/cssc.201702139

S. Honda, M. Katayama, K.-Y. Lee et al., Low temperature synthesis of aligned carbon nanotubes by inductively coupled plasma chemical vapor deposition using pure methane. Jpn J. Appl. Phys. **42**, L441 (2003). https://doi.org/10.1143/JJAP.42.L441

W.S. Hummers, R.E. Offeman, Preparation of graphitic oxide. J. Am. Chem. Soc. **80**, 1339 (1958). https://doi.org/10.1021/ja01539a017

M. Huskić, D. Kepić, D. Kleut et al., The Influence of Reaction Conditions on the Properties of Graphene Oxide. Nanomaterials **14**, (2024)https://doi.org/10.3390/nano14030281

J. Janca, M. Elias, V. Brozek, Precursors in Inductive RF Discharge Plasma Reactors, Reduction of Tungsten. High. Temp. Mater. Process. Int. Q. High-Technology Plasma Process. **7**, 357–366 (2003)

P.J. Jesuraj, R. Parameshwari, K. Jeganathan, Improved performance of graphene oxide based resistive memory devices through hydrogen plasma. Mater. Lett. **232**, 62–65 (2018). https://doi.org/10.1016/j.matlet.2018.08.073

M. Jovičević-Klug, I.R. Souza Filho, H. Springer et al., Green steel from red mud through climate-neutral hydrogen plasma reduction. Nature. **625**, 703–709 (2024). https://doi.org/10.1038/s41586-023-06901-z

I. Jung, D.A. Dikin, R.D. Piner, R.S. Ruoff, Tunable electrical conductivity of individual graphene oxide sheets reduced at low temperatures. Nano Lett. **8**, 4283–4287 (2008). https://doi.org/10.1021/nl801938

Z. Ke, Y. Ma, Z. Zhu et al., Non-thermal hydrogen plasma processing effectively increases the antibacterial activity of graphene oxide. Appl. Phys. Lett. **112** (2018). https://doi.org/10.1063/1.5012132
K. Kosaentor, C. Chaiwong, Reduction of graphene oxide via plasma immersion ion implantation. Plasma Chem. Plasma Process. 33–47 (2024). https://doi.org/10.1007/s11090-024-10513-4
R.K. Kroon, Removal of Removal of oxygen from the Si(100) surface in a DC hydrogen plasma. Jpn J. Appl. Phys. **36**, 5068 (1997). https://doi.org/10.1143/JJAP.36.5068
A. Kurtishaj Hamzaj, E. Donà, M. Santhosh N, et al., Plasma-modification of graphene oxide for advanced ammonia sensing. Appl. Surf. Sci. **660**, 1–11 (2024). https://doi.org/10.1016/j.apsusc.2024.160006
X. Li, G. Zhang, X. Bai et al., Highly conducting graphene sheets and Langmuir–Blodgett films. Nat. Nanotechnol. **3**, 538–542 (2008). https://doi.org/10.1038/nnano.2008.210
K. Li, Z. Cai, M. Li et al., Direct growth of nanographene at low temperature from carbon black for highly sensitive temperature detectors. Nanotechnology. **27** (2016). https://doi.org/10.1088/0957-4484/27/50/505603
J.L. Liu, S. Liu, J.C. Guo et al., Formation mechanism of the H-terminated diamond surface. Wuli Huaxue Xuebao. Acta Phys. - Chim. Sin. **31**, 1741–1746 (2015). https://doi.org/10.3866/PKU.WHXB201508031
X. Liu, X. He, Y. Lin et al., Enhanced adhesion strength and solid lubricity of graphite like amorphous carbon films by hydrogen implantation. Surf. Coat. Technol. **412**, 127013 (2021). https://doi.org/10.1016/j.surfcoat.2021.127013
L. Long, W. Zhou, J. Tang, D. Zhou, Experiment study on etching process of graphite electrode by DC hydrogen plasma. Plasma Process. Polym. **17**, 1–10 (2020). https://doi.org/10.1002/ppap.201900242
M. Magureanu, N.B. Mandache, C. Rizescu et al., Engineering hydrogenation active sites on graphene oxide and N-doped graphene by plasma treatment. Appl. Catal. B Environ. **287**, 119962 (2021). https://doi.org/10.1016/j.apcatb.2021.119962
G.A. Melin, R.J. Madix, Energy accommodation during hydrogen atom recombination on metal surfaces. Trans. Faraday Soc. **67**, 2711–2719 (1971). https://doi.org/10.1039/TF9716702711
I. Méndez, F.J. Gordillo-Vázquez, V.J. Herrero, I. Tanarro, Atom and ion chemistry in low pressure hydrogen DC plasmas. J. Phys. Chem. A **110**, 6060–6066 (2006). https://doi.org/10.1021/jp057182+
M. Mozetic, A. Zalar, Recombination of neutral hydrogen atoms on AISI 304 stainless steel surface. 399–403 (1999)
M. Mozetič, Low – pressure non – equilibrium plasma technologies: scientific background and technological challenges (Springer Nature Singapore) (2025)
M. Mozetič, A. Vesel, G. Primc, R. Zaplotnik, Introduction to Plasma and Plasma Diagnostics, in Non-Thermal Plasma Technology for Polymeric Materials, ed. by S. Thomas, M. Mozetič, U. Cvelbar et al. (Elsevier) pp. 23–65 (2019)
S. Muhammad Hafiz, R. Ritikos, T.J. Whitcher et al., A practical carbon dioxide gas sensor using room-temperature hydrogen plasma reduced graphene oxide. Sens. Actuators B Chem. **193**, 692–700 (2014). https://doi.org/10.1016/j.snb.2013.12.017
R.R. Nair, P. Blake, A.N. Grigorenko et al., Fine structure constant defines visual transparency of graphene. **320** (2008)
K.S. Novoselov, A.K. Geim, S.V. Morozov, D. Jiang, Y. Zhang, S.V. Dubonos, et al., Electric field effect in atomically thin carbon films. Science. **306** 666–669 (2004)
W.K. Park, Y. Yoon, Y. Hyun et al., High-efficiency exfoliation of oxide with controlled dimension. Sci. Rep. 1–9 (2017). https://doi.org/10.1038/s41598-017-16649-y
J. Petucci, S. Semone, C. LeBlond et al., Formation of H2 on graphene using Eley-Rideal and Langmuir-Hinshelwood processes. J. Chem. Phys. **149**, 14702 (2018). https://doi.org/10.1063/1.5026691
G. Primc, Generation of neutral chemically reactive species in low-pressure plasma. Front. Phys. **10**, 1–8 (2022). https://doi.org/10.3389/fphy.2022.895264
A. Primo, A. Franconetti, M. Magureanu et al., Engineering active sites on reduced graphene oxide by hydrogen plasma irradiation: mimicking bifunctional metal/supported catalysts in hydrogenation reactions. Green. Chem. **20**, 2611–2623 (2018). https://doi.org/10.1039/c7gc03397d
I. Sengupta, S. Chakraborty, M. Talukdar et al., Thermal reduction of graphene oxide: how temperature influences purity. J. Mater. Res. **33**, 4113–4122 (2018). https://doi.org/10.1557/jmr.2018.338
Y. Seon Lee, N. Ryeol Kim, S. Ki Park et al., Effects of high-temperature thermal reduction on thermal conductivity of reduced graphene oxide polymer composites. Appl. Surf. Sci. **650**, 159140 (2024). https://doi.org/10.1016/j.apsusc.2023.159140

G. Singh, V.D. Botcha, D.S. Sutar et al., Near room temperature reduction of graphene oxide Langmuir-Blodgett monolayers by hydrogen plasma. Phys. Chem. Chem. Phys. **16**, 11708–11718 (2014). https://doi.org/10.1039/c4cp00875h

M. Torabi, R. Karimi Shervedani, A. Amini, High performance porous graphene nanoribbons electrodes synthesized via hydrogen plasma and modified by Pt-Ru nanoclusters for charge storage and methanol oxidation. Electrochim. Acta. **290**, 616–625 (2018). https://doi.org/10.1016/j.electacta.2018.09.082

A. Vesel, R. Zaplotnik, G. Primc, M. Mozetič, Synthesis of vertically oriented graphene sheets or carbon nanowalls-review and challenges. Mater. (Basel). **12** (2019). https://doi.org/10.3390/ma12182968

A. Vesel, R. Zaplotnik, G. Primc, M. Mozetic, Fundamentals of thin film depth profiling by glow discharge optical emission spectroscopy. J. Vac Sci. Technol. A **41** (2023). https://doi.org/10.1116/6.0002695

J.J. Wang, M.Y. Zhu, R.A. Outlaw et al., Free-standing subnanometer graphite sheets. Appl. Phys. Lett. **85**, 1265–1267 (2004). https://doi.org/10.1063/1.1782253

C. Yang, J. Gong, P. Zeng et al., Fast room-temperature reduction of graphene oxide by methane/argon plasma for flexible electronics. Appl. Surf. Sci. **452**, 481–486 (2018). https://doi.org/10.1016/j.apsusc.2018.04.272

S. Yonemura, K. Nanbu, Dc self-bias voltages in radio frequency magnetron discharges. Thin Solid Films. **506–507**, 517–521 (2006). https://doi.org/10.1016/j.tsf.2005.08.111

R. Zaplotnik, G. Primc, D. Paul, M. Mozetič, J. Kovač, AV, Atomic species generation by plasmas. In: Plasma Applications for Material Modification. p 70 (2021)

X. Zhang, H. Liu, Q. Lou et al., Hydrogen plasma on graphene oxide to produce gradients of oxygen-containing functional groups for self-powered devices. ACS Appl. Nano Mater. **5**, 16664–16673 (2022). https://doi.org/10.1021/acsanm.2c03690

J. Zhang, Z. Peng, T. Zhang et al., Hydrogen plasma reduction of iron oxides. Int. J. Hydrogen Energy. **105**, 910–920 (2025). https://doi.org/10.1016/j.ijhydene.2025.01.322